NASA Technical Memorandum 85980

Simulation of Transonic Separated Airfoil Flow by Finite-Difference Viscous-Inviscid Interaction

William R. Van Dalsem and Joseph L. Steger

June 1984

National Aeronautics and
Space Administration

NASA Technical Memorandum 85980

Simulation of Transonic Separated Airfoil Flow by Finite-Difference Viscous-Inviscid Interaction

William R Van Dalsem
Joseph L Steger, Ames Research Center, Moffett Field, California

National Aeronautics and
Space Administration

Ames Research Center
Moffett Field, California 94035

SIMULATION OF TRANSONIC SEPARATED AIRFOIL FLOW BY FINITE-DIFFERENCE VISCOUS-INVISCID INTERACTION

William R. Van Dalsem and Joseph L. Steger
Ames Research Center, NASA
Moffett Field, California

INTRODUCTION

A finite-difference viscous-inviscid interaction program has been developed for simulating the separated transonic flow about lifting airfoils, including the wake. In contrast to most interaction programs, this code combines a finite-difference boundary-layer algorithm with the inviscid program. The recently developed finite-difference boundary-layer code efficiently simulates attached and reversed compressible boundary-layer and wake flows. New viscous-inviscid interaction algorithms were also developed to couple the boundary-layer code and the inviscid transonic full-potential program (see ref. [1] for details). Transonic cases with shock-induced and trailing-edge separation are computed and compared with experimental and Navier-Stokes results.

VISCOUS ALGORITHM

The compressible boundary-layer equations for the steady, two-dimensional flow of a perfect gas are written in $\xi(x),\eta(x,y)$ coordinates:

$$\rho[u(u_\xi \xi_x + u_\eta \eta_x) + v u_\eta \eta_y] = -\beta p_\xi \xi_x + (\mu u_\eta \eta_y)_\eta \eta_y \tag{1a}$$

$$\rho c_p[u(T_\xi \xi_x + T_\eta \eta_x) + v T_\eta \eta_y] = \beta u p_\xi \xi_x + (\kappa T_\eta \eta_y)_\eta \eta_y + \mu(u_\eta \eta_y)^2 \tag{1b}$$

$$(\rho u)_\xi \xi_x + (\rho u)_\eta \eta_x + (\rho v)_\eta \eta_y = 0 \tag{1c}$$

where the equations are nondimensionalized as outlined in references [2-3]. By using a general x,y to ξ,η coordinate transformation, a complex similarity transformation is avoided and a solution-adaptive grid is easily employed. In this work, the grid height is varied as a function of the computed displacement thickness.

Near and in reversed-flow regions, the boundary-layer equations are solved in the inverse mode to avoid singular behavior at the separation point. Here the wall shear stress τ_w and the wake centerline velocity u_{wc} are used as the inverse forcing functions because they are efficiently implemented in the following numerical algorithm.

The boundary-layer equations are solved using an implicit predictor-corrector algorithm. Streamwise marching begins by predicting estimates of u, T, ρ, v, μ, and κ. This predictor step uses first-order ξ operators in the x-momentum and energy equations, but for one step produces second-order accurate values. Because the predictor step only needs to be first-order accurate, any nonlinear coefficients can be lagged in ξ. A second-order accurate corrector step is then used to calculate improved values of u, T, ρ, v, μ, and κ. During the corrector step, the nonlinear coefficients are evaluated using the most recently computed flow variables. Overall, second-order accurate solutions are obtained at the cost of two scalar bidiagonal and four scalar tridiagonal matrix inversions per streamwise station.

The algorithm is presented below in operator notation, where E is the shift operator (e.g., $E_\xi^{-1} u_j = u_{j-1}$):

$$\nabla_\xi = (1 - E_\xi^{-1})/(\Delta\xi) \qquad \Delta_\xi = (E_\xi^{+1} - 1)/(\Delta\xi)$$

$$\delta_\xi = (E_\xi^{+1} - E_\xi^{-1})/(2\Delta\xi) \qquad \bar{\delta}_\xi = (E_\xi^{+\frac{1}{2}} - E_\xi^{-\frac{1}{2}})/(\Delta\xi)$$

A predictor-step result is denoted by a tilde (e.g., $\tilde{u}$) and, unless indicated otherwise, the indices are j,k. The superscripts I, II, and III denote flow-dependent operations.

Predictor Step

Predict $\tilde{u}$ at the new station using the x-momentum equation

$$(\rho u)_{j+s'}(\xi_x \delta'_\xi \tilde{u} + \eta_x \delta_\eta \tilde{u}) + (\rho v)_{j+s'}(\eta_y \delta_\eta \tilde{u}) = -\beta \xi_x \delta_\xi p + \eta_y \bar{\delta}_\eta (\mu_{j+s'} \eta_y \bar{\delta}_\eta \tilde{u}) \quad (2a)$$

Predict $\tilde{T}$ at the new station using the energy equation

$$\rho_{j+s'} c_p [\tilde{u}(\xi_x \delta'_\xi \tilde{T} + \eta_x \delta_\eta \tilde{T}) + v_{j+s'} \eta_y \delta_\eta \tilde{T}] = \beta \tilde{u} \xi_x \delta_\xi p + \eta_y \bar{\delta}_\eta (\kappa_{j+s'} \eta_y \bar{\delta}_\eta \tilde{T}) + \mu_{j+s'} (\eta_y \delta_\eta \tilde{u})^2 \quad (2b)$$

Obtain $\tilde{\rho} = p/\tilde{T}$ and integrate the continuity equation for $\tilde{v}$

$$\nabla_\eta (\tilde{\rho}\tilde{v}) = -\frac{1 + E_\eta^{-1}}{2} \frac{\xi_x \delta'''_\xi (\tilde{\rho}\tilde{u}) + \eta_x \delta_\eta (\tilde{\rho}\tilde{u})}{\eta_y} \quad (2c)$$

The coefficients $\tilde{\mu}$ and $\tilde{\kappa}$ are then evaluated using the Cebeci turbulence model [4].

Corrector Step

Correct u at the new station using the x-momentum equation

$$\tilde{\rho}\tilde{u}(\xi_x \delta''_\xi u + \eta_x \delta_\eta u) + \tilde{\rho}\tilde{v}(\eta_y \delta_\eta u) = -\beta \xi_x \delta_\xi p + \eta_y \bar{\delta}_\eta (\tilde{\mu} \eta_y \bar{\delta}_\eta u) \quad (3a)$$

Correct T at the new station using the energy equation

$$\tilde{\rho} c_p [u(\xi_x \delta''_\xi T + \eta_x \delta_\eta T) + \tilde{v}(\eta_y \delta_\eta T)] = \beta u \xi_x \delta_\xi p + \eta_y \bar{\delta}_\eta (\tilde{\kappa} \eta_y \bar{\delta}_\eta T) + \tilde{\mu} (\eta_y \delta_\eta u)^2 \quad (3b)$$

Update ρ, v, μ, and κ as before.

Flow-dependent operators are used near reversed flow. The logic for determining the appropriate operators by specifying values of s' and s is summarized in figure 1. To incorporate the flow-dependent differencing, the operators $\delta_\xi{}'$, $\delta_\xi{}''$, and $\delta_\xi{}'''$ are defined as

$$\delta'_\xi = \begin{cases} \nabla_\xi \\ \delta_\xi \\ \Delta_\xi \end{cases} \qquad \delta''_\xi = \begin{cases} \nabla_\xi (3 - E_\xi^{-1})/2 & s = -1 \\ \delta_\xi & s = 0 \\ \Delta_\xi (3 - E_\xi^{+1})/2 & s = 1 \end{cases} \quad (4)$$

$$\delta'''_\xi = \begin{cases} \nabla_\xi (3 - E_\xi{}^{-1})/2 & s' = -1 \\ \delta_\xi & s' = 0 \end{cases}$$

When using flow-dependent differencing values at $j + 1$ and $j + 2$ are obtained from a previous iterative sweep. Sweeping of the viscous flow is already required by the viscous-inviscid iterations.

The algorithm is modified to operate in the inverse mode by replacing the pressure term in the x-momentum equation with expressions containing the inverse forcing functions. These relations are obtained by applying the x-momentum equation at the wall and wake centerline. For example, at a wall ($k = 1$) the x-momentum equation yields an equality between the pressure term and the viscous term evaluated at the wall. Replacing the pressure term with a difference approximation of the viscous term in, for example, the corrector step x-momentum difference equation yields

$$\tilde{\rho}\tilde{u}(\xi_x \delta''_\xi u + \eta_x \delta_\eta u) + \tilde{\rho}\tilde{v}(\eta_y \delta_\eta u) = -2 \frac{\frac{\tilde{\mu}_2 + \tilde{\mu}_1}{2} \frac{u_2}{y_2} - \tau_w}{y_2} + \eta_y \bar{\delta}_\eta (\tilde{\mu} \eta_y \bar{\delta}_\eta u) \quad (5)$$

A similar adaptation is made in the wake.

Equation (5) shows that in the inverse mode u_2 appears in the difference equation at every k index. If this term is treated implicitly, a tridiagonal-like matrix with an additional column of nonzero coefficients is obtained. This augmented scalar tridiagonal matrix system is efficiently solved using an LU decomposition algorithm (see refs. [2-3]). Because the inverse forcing functions are implemented implicitly, no iteration is required to obtain the desired τ_w or u_{wc}.

VISCOUS-INVISCID INTERFACES

If τ_w falls below a prescribed value the viscous algorithm converts from the direct to the inverse mode from that point on, including the entire wake. When operating in the inverse mode τ_w or u_{wc} must be updated so the viscous and inviscid pressures converge. A number of schemes for updating τ_w and u_{wc} were studied. The following are the fastest and most reliable of those studied and were used to obtain all the presented results:

$$\tau_w^{n+1} = \tau_w^n + \omega(p_v^n - p_i^{n+1}) \qquad \text{where:} \quad \omega = 10 \tag{6a}$$

$$u_{wc}^{n+1} = u_{wc}^n + \omega_c(p_v^n - p_i^{n+1}) \qquad \omega_c = 2 \tag{6b}$$

A transpiration velocity [5] is used to introduce the influence of the viscous region upon the inviscid flow. After δ^* has been calculated the transpiration velocity is computed and then converted to the required perturbations of the inviscid contravariant velocities used in the inviscid algorithm. This approach allows the use of inviscid grids that are not orthogonal to a body surface or wake centerline in interaction codes

In many cases it is necessary to account for the viscous flow curvature and the pressure jump that occurs across these curved stream-tubes. Therefore, the method of accounting for the pressure variation across the shear layers developed by Lock and Firmin [6] is incorporated into the present algorithm The reader is referred to reference [3] for details.

RESULTS

The interaction code was first tested by comparison with Navier-Stokes computations [7] of the $M_\infty = 0.720$ flow past an 18% biconvex airfoil. The agreement between the present results and the free-flight results of Levy is good in terms of both the computed pressure distributions (see fig. 2) and separation points. Also shown are experimental data [8] and the results of Levy's calculations which include the tunnel walls. It is apparent that the experimental data were affected by the tunnel walls Experimental data and computational results are also available for this airfoil at $M_\infty = 0.754$. Experimentally, this flow can be unsteady unless a trailing-edge splitter plate is installed, which is modeled in the computations. As shown in figure 3, there is some shock-position discrepancy between the present computations and the experimental data and results of Levy; it is attributed to the wind-tunnel wall effects. Otherwise, the present results are in good agreement with the Navier-Stokes results. Both computations predict a greater trailing-edge pressure recovery than observed experimentally The computed C_f distribution for this case (see fig. 4) indicates that shock-induced and trailing-edge separation are predicted. To indicate the convergence rate, the $C_{f\,min}$ history for these cases is presented in figure 5. The $M_\infty = 0.720$ case has converged by the 75th iteration, whereas because of the strong shock-separated boundary-layer interaction, the $M_\infty = 0.754$ case requires approximately 160 iterations to converge.

McDevitt [9] also measured M_{peak} on the 18% biconvex (with trailing-edge splitter plate) versus M_∞. Figure 6 compares the results of the present method to this experimental data. The comparison is encouraging, especially considering the tunnel-wall effects on

this data. Also, at the higher Mach numbers some of the discrepancy may be due to the isentropic inviscid flow assumption. The large difference between the inviscid and viscous peak Mach numbers is indicative of the strong viscous-inviscid interaction being modeled.

To verify the treatment of lifting airfoils, the results of computing the $M_\infty = 0.8$ flow about a NACA 0012 at $\alpha = 1°$ are compared with experimental data [10] and Navier-Stokes [11] results. Figure 7 shows good agreement between the experimental and computed C_p distributions. Both computations predict shock-induced separation from approximately 56% to 67% of chord and trailing-edge separation from 95% of chord.

As a final case, the results of computing the $M_\infty = 0.73$ flow about the RAE 2822 airfoil at $C_l = 0.803$ are presented. Figures 8-10 compare the $C_p, C_f|_e$, and δ^* distributions found experimentally [12], those computed by the present method, and those computed by Mehta [13] using a Navier-Stokes code. Mehta performed his computations at $\alpha = 2.79°$ (and computed a $C_l = 0.793$); the present computations were performed at $\alpha = 2.81°$ to match the measured $C_l = 0.803$. The present results are in good agreement with both the Navier-Stokes and experimental results. The velocity vectors near the trailing edge computed by the present method are presented in figure 11. This figure indicates the high resolution obtainable.

These simulations were obtained on 223x31 inviscid and 223x50 viscous grids. For the cases presented, the required Cray-XMP CPU time was 7 to 15 sec, and on the average, 0.0006 sec/grid point were required to obtain a converged solution In contrast, an optimized version of the thin-layer Navier-Stokes code developed by Steger and Pulliam [11] requires about 0.06 sec/grid point to obtain a converged solution

SUMMARY

A fast, versatile, direct-inverse finite-difference boundary-layer code has been developed and coupled to a transonic full-potential airfoil code via new viscous-inviscid interaction algorithms. The developed interaction code has been used to compute non-lifting and lifting separated transonic airfoil flows, and the results are in good agreement with experimental data and Navier-Stokes computations. Furthermore, the cost of these solutions is less than twice the cost of the inviscid solutions and close to two orders-of-magnitude less than Navier-Stokes solutions.

REFERENCES

1. Holst, T. L., **AIAA Journal**, Vol. 17, Oct. 1979, pp. 1038-1045.
2. Van Dalsem, W. R., and Steger, J. L., AIAA Paper No 83-1689.
3 Van Dalsem W. R., Ph.D. Thesis, Stanford University, Jun. 1984.
4. Cebeci, T., AIAA Paper No. 70-741.
5. Lighthill, M. J., **Journal of Fluid Mechanics**, Vol. 4, 1958, pp. 383-392.
6. Lock, R. C., and Firmin, M. C. P., RAE Technical Memo. 1900, Apr. 1981.
7. Levy, L. L., **AIAA Journal**, Vol. 16, Jun. 1978, pp. 564-572.
8. McDevitt, J. B., Levy, L. L., and Deiwert, G. S., AIAA Paper No. 75-878.
9. McDevitt, J. B., NASA TM-78549, Jan. 1979.
10. Whitfield, J. D., et al., **Computers and Fluids**, Vol. 8, 1980, pp. 71-99.
11. Pulliam, T. H., CFD User's Workshop, Tullahoma, Tenn., Mar. 1984.
12. Cook, P. H., McDonald, M. A., and Firmin, M. C. P., AGARD AR 138, 1979.
13. Mehta, U., Second Symposium on Aerodynamic Flows, Jan. 17-20, 1983.

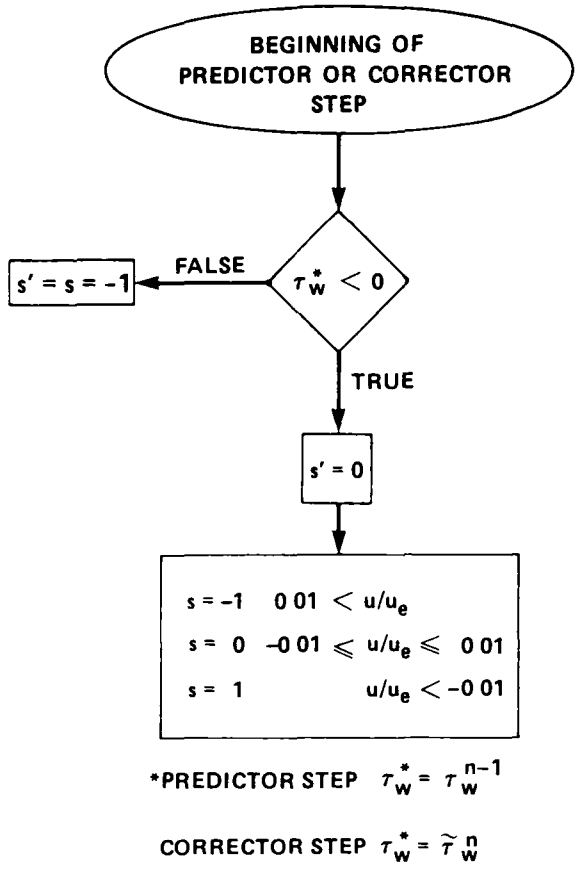

Fig. 1 Flow-dependent differencing logic.

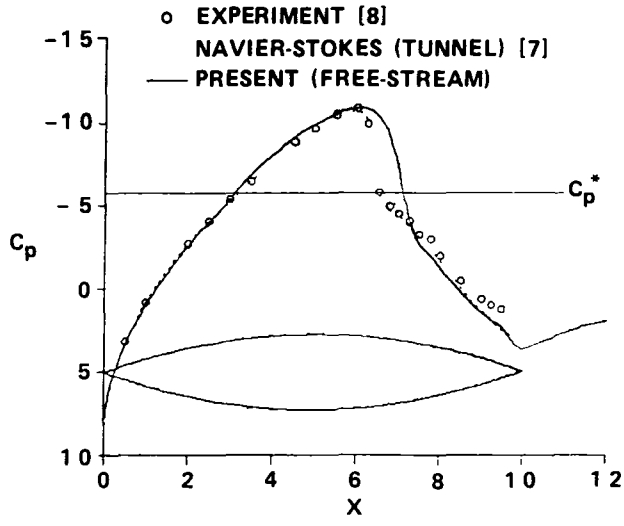

Fig. 3 C_p distributions for an 18% biconvex at $M_\infty = 0.754, Re_\infty = 8x10^6$

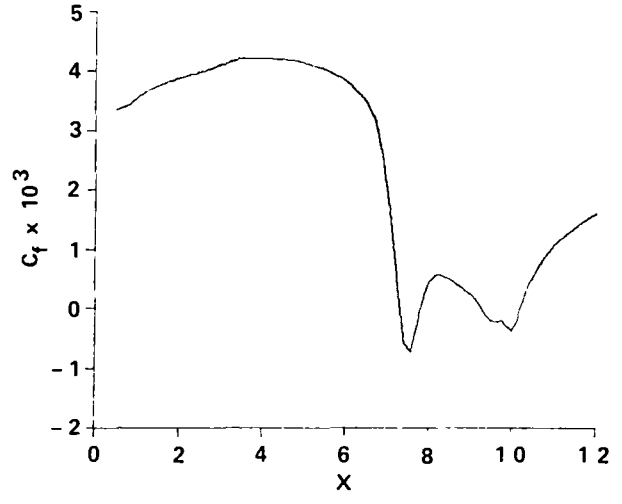

Fig. 4 Computed C_f distribution for an 18% biconvex at $M_\infty = 0.754$, $Re_\infty = 8x10^6$

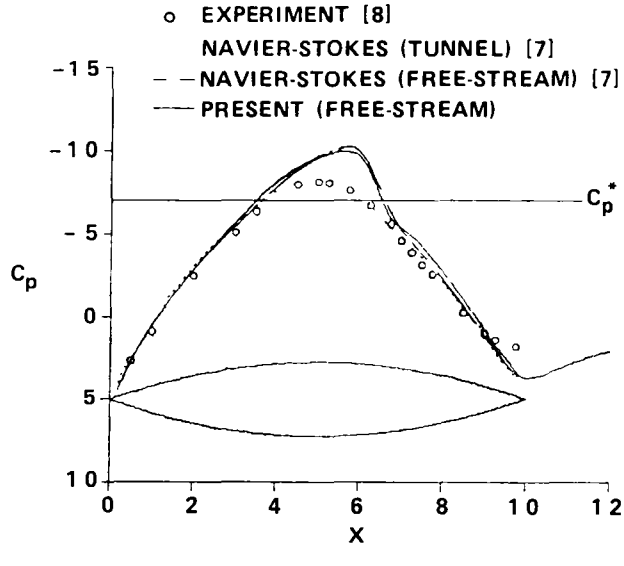

Fig 2 C_p distributions for an 18% biconvex at $M_\infty = 0.720, Re_\infty = 11x10^6$.

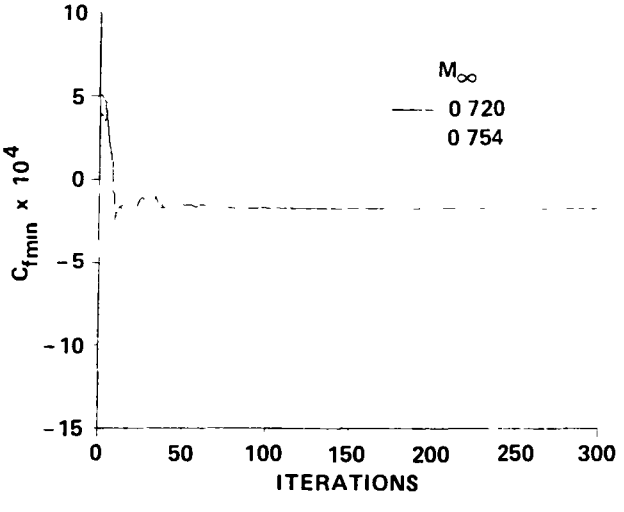

Fig. 5 Minimum C_f history for the $M_\infty = 0.720$, $Re_\infty = 11x10^6$ and $M_\infty = 0.754$, $Re_\infty = 8x10^6$ solutions

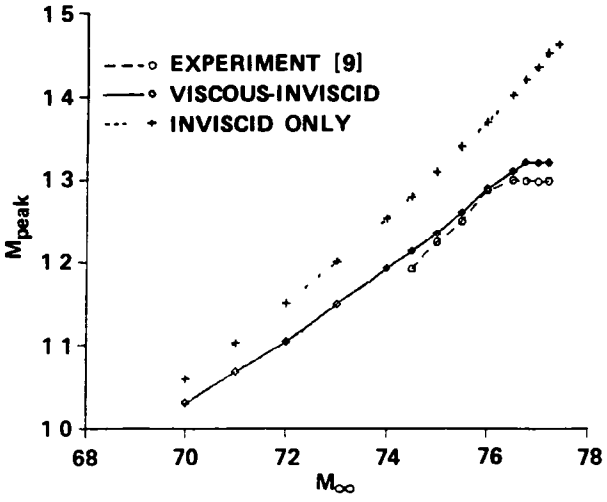

Fig. 6 M_{peak} versus M_∞ for the $Re_\infty = 8x10^6$ flow about an 18% biconvex.

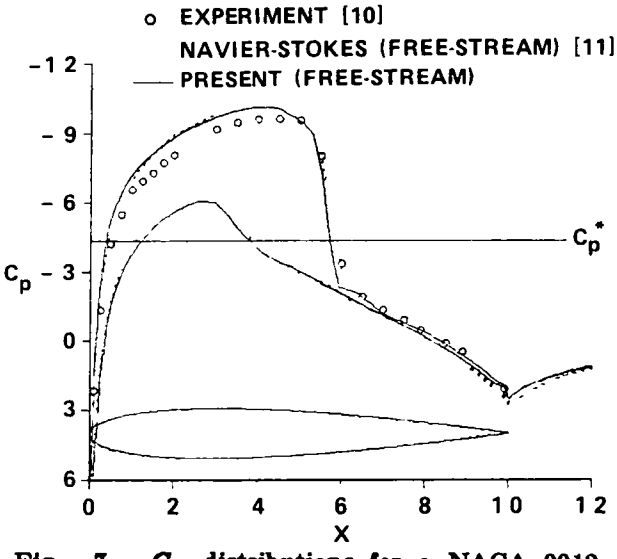

Fig. 7 C_p distributions for a NACA 0012 airfoil at $M_\infty = 0.800, Re_\infty = 2.25x10^6$, $\alpha = 1^\circ$

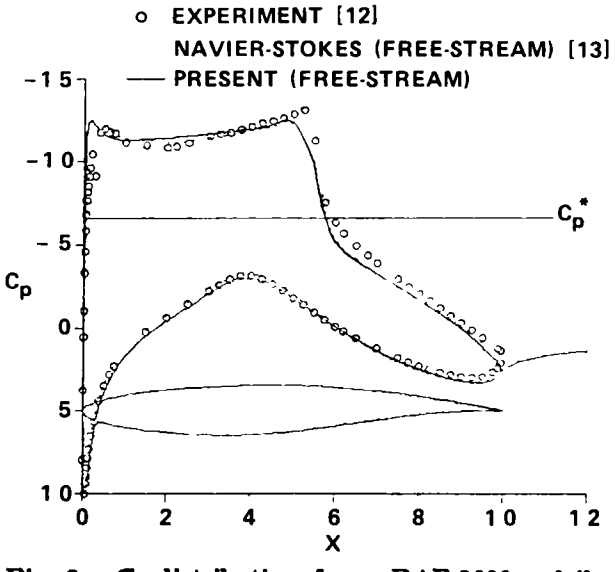

Fig. 8 C_p distributions for an RAE 2822 airfoil at $M_\infty = 0.730, Re_\infty = 6.50x10^6, C_l = 0.803$

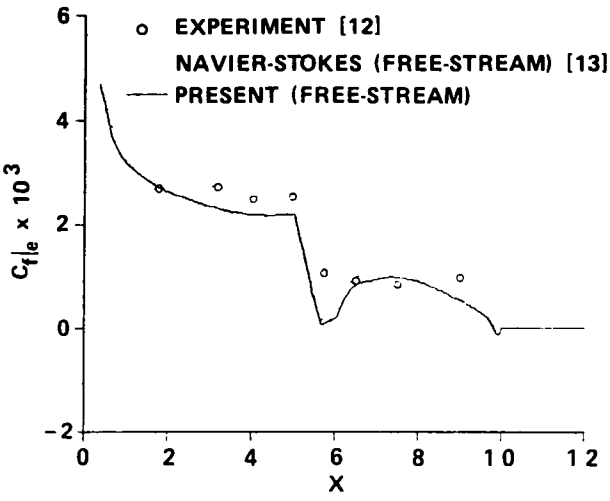

Fig. 9 $C_f|_e$ distributions for an RAE 2822 airfoil at $M_\infty = 0.730, Re_\infty = 6.50x10^6$, $C_l = 0.803$.

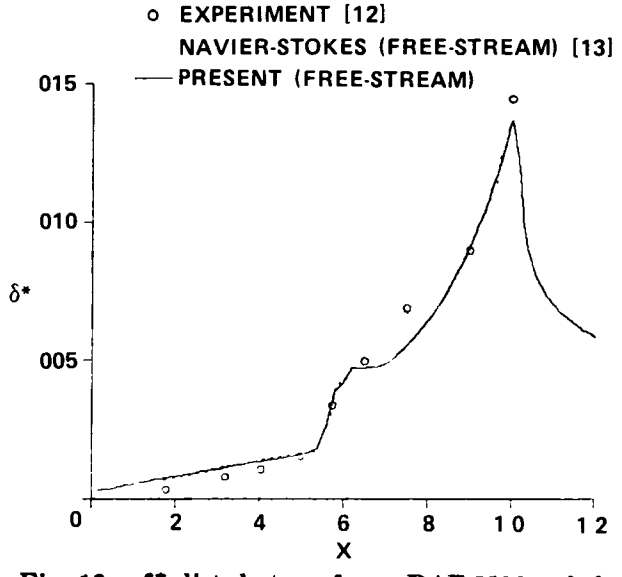

Fig. 10 δ^* distributions for an RAE 2822 airfoil at $M_\infty = 0.730, Re_\infty = 6.50x10^6, C_l = 0.803$

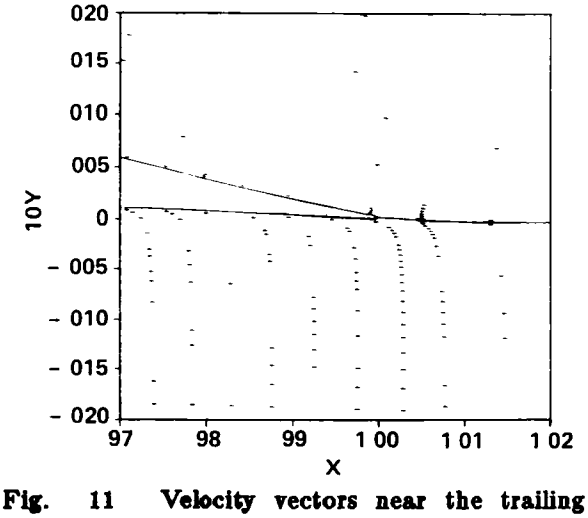

Fig. 11 Velocity vectors near the trailing edge of an RAE 2822 airfoil at $M_\infty = 0.730$, $Re_\infty = 6.50x10^6, C_l = 0.803$.

1 Report No	2 Government Accession No	3 Recipient's Catalog No
NASA Technical Memorandum	85980	

4 Title and Subtitle	5 Report Date
SIMULATION OF TRANSONIC SEPARATED AIRFOIL FLOW BY FINITE DIFFERENCE VISCOUS-INVISCID INTERACTION	June 1984
	6 Performing Organization Code
7 Author(s)	8 Performing Organization Report No
William R. Van Dalsem and Joseph L. Steger	A-9812
	10 Work Unit No
9 Performing Organization Name and Address	T-6458
Ames Research Center Moffett Field, CA 94035	11 Contract or Grant No
	13 Type of Report and Period Covered
12 Sponsoring Agency Name and Address	Technical Memorandum
National Aeronautics and Space Administration Washington DC, 20546	14 Sponsoring Agency Code 505-13

15 Supplementary Notes

Point of contact: William R. Van Dalsem, Ames Research Center, MS 202A-14, Moffett Field, CA 94035 (415) 965-6741 or FTS 448-6741

16 Abstract

A finite-difference viscous-inviscid interaction program has been developed for simulating the separated transonic flow about lifting airfoils, including the wake. In contrast to most interaction programs, this code combines a finite-difference boundary-layer algorithm with the inviscid program. The recently developed finite-difference boundary layer code efficiently simulates attached and reversed compressible boundary-layer and wake flows. New viscous-inviscid interaction algorithms were also developed to couple the boundary-layer code with the inviscid transonic full-potential program. Transonic cases with shock-induced and trailing-edge separation are computed and compared with experimental and Navier-Stokes results.

17 Key Words (Suggested by Author(s))	18 Distribution Statement
Transonic separated airfoil flow Viscous-inviscid interaction Finite-difference	Unlimited Subject category - 02

19 Security Classif (of this report)	20 Security Classif (of this page)	21 No of Pages	22 Price*
Uncl.	Uncl.	9	A02

*For sale by the National Technical Information Service, Springfield, Virginia 22161

End of Document